Supplementary Material

Sketch diagrams of SnO_2 and TiO_x deposition are shown in Fig. S1. SnO_2 was deposited on Si wafer via a chemical vapor deposition (CVD) method. Si wafer and $SnCl_2$ powder was placed in middle of the tube. Sublimated $SnCl_2$ was deposited on Si wafer under air flow, during which $SnCl_2$ was converted to SnO_2. TiO_x was deposited by pumping titanium tetraisopropanolate into the tube with N_2 flow to deposit on Si-SnO_2 surface.

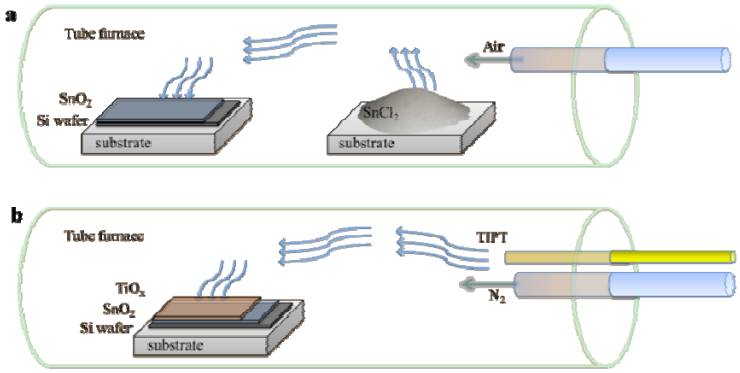

Fig. S1 Sketch diagrams of (a) SnO_2 and (b) TiO_x deposition

SEM images of Si-SnO_2 prepared with 0.01 g and 0.10 g $SnCl_2$ are shown in Fig. S2. When 0.01 g $SnCl_2$ is applied, only a few particles are dispersed on Si surface. However, 0.10 g $SnCl_2$ leads to thicker SnO_2 film.

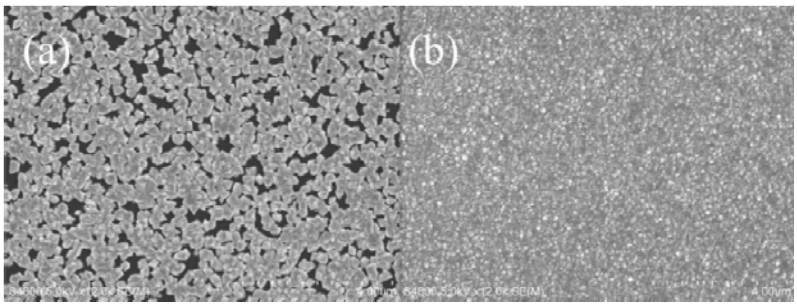

Fig. S2 SEM images of Si-SnO_2 ((a) 0.01 g $SnCl_2$ and (b) 0.10 g $SnCl_2$)

Elemental mapping of Si-SnO_2-TiO_x (top view) is shown in Fig. S3 and the well-distributed Si, Sn, Ti and O dots prove SnO_2 and TiO_x both deposited on Si wafer uniformly.

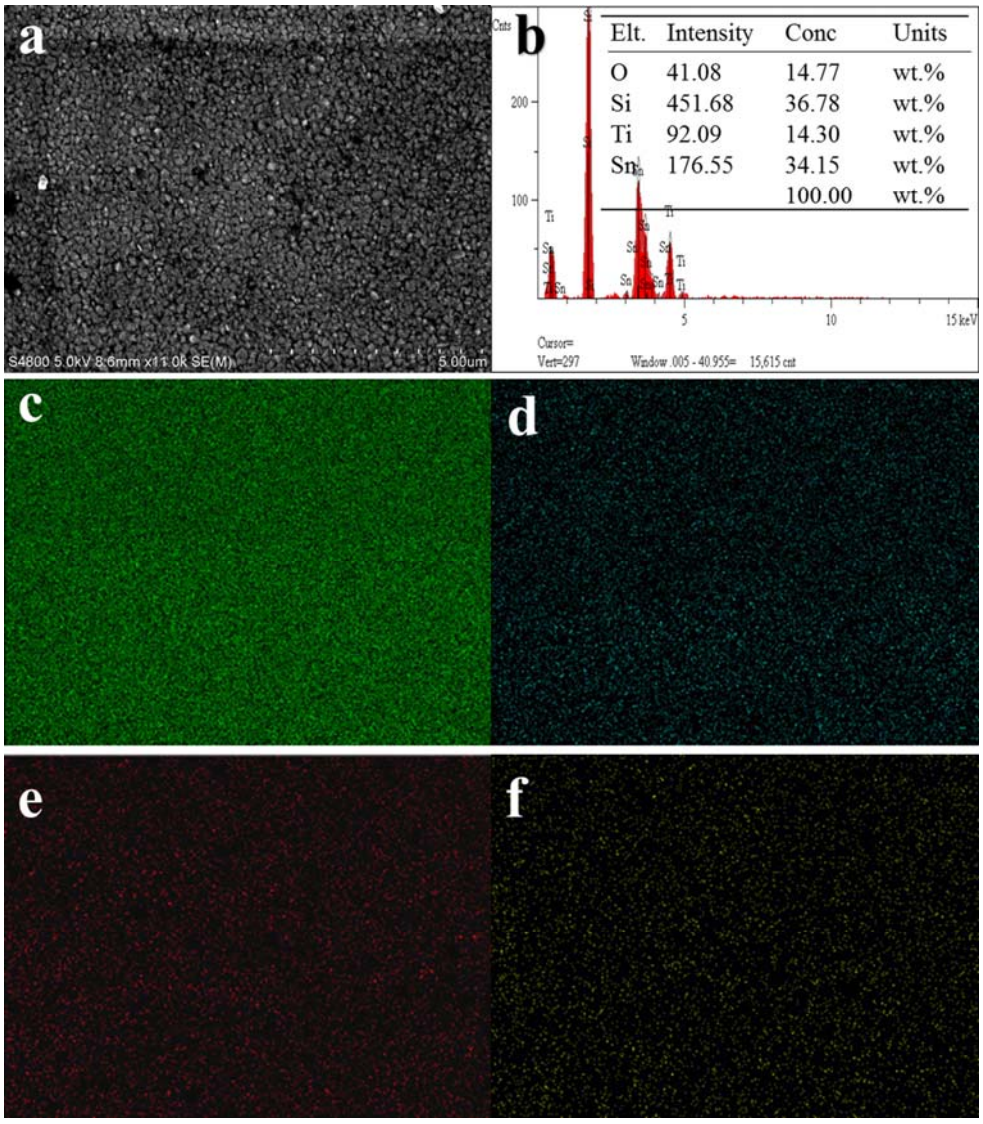

Fig. S3 (a) SEM images of Si-SnO_2-TiO_x, (b) EDX spectrum and element mapping of (c) Si, (d) Sn, (e) Ti and (f) O

Structural characterizations of SnO_2 and TiO_x are revealed by FTIR spectra (Fig. S4).

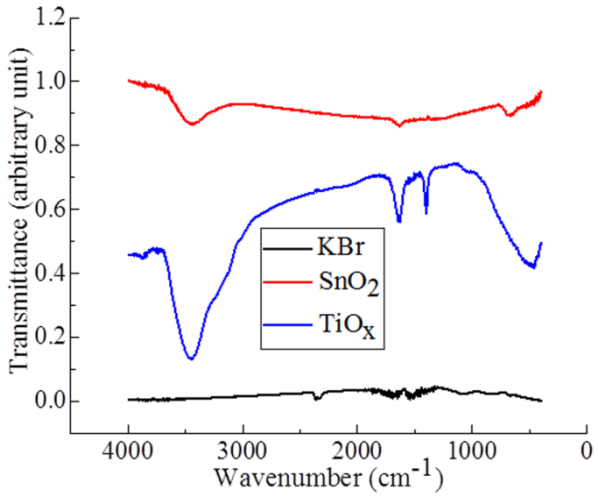

Fig. S4 FTIR spectra of SnO_2 and TiO_x

Magnified photocurrent response of Si from Fig. 4(e) is shown in Fig. S5.

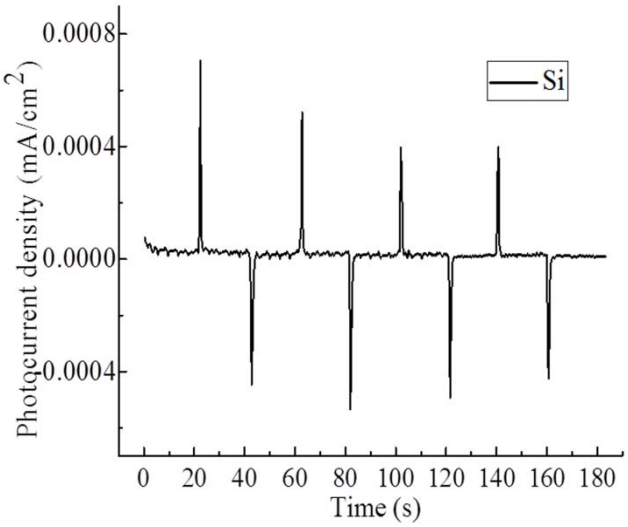

Fig. S5 Magnified photocurrent response of Si

Open circuit voltages (Voc) of the as-prepared samples are measured under intermittent UV/vis light (Fig. S6). Open circuit voltages (Voc) of the as-prepared samples are measured under intermittent UV/vis light.

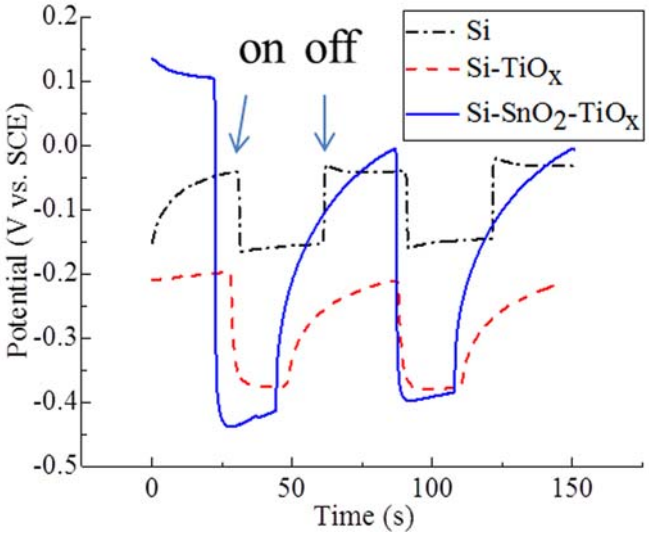

Fig. S6 V_{oc} tests of Si, Si-TiO_x and Si-SnO_2-TiO_x

To further confirm the existence of ·OH and $\cdot O_2^-$, the electron spin resonance (ESR) experiments were carried out on an ESR spectrometer (A200, Bruker). A 50 mmol/L 5, 5-dimethyl-1-pyrroline-N-oxide (DMPO) solution was used as radical trapping reagent (in water for ·OH and in methanol for $\cdot O_2^-$). Si-SnO_2-TiO_x electrode and Pt electrode were separated by Nafion 117 film in a double cell and connected by wire. The DMPO-·OH and DMPO-$\cdot O_2^-$ signals of the electrodes are illustrated in Fig. S7. A 1:2:2:1 signal of DMPO-·OH is observed in both cells, proving ·OH radicals generate on Si-SnO_2-TiO_x electrode and Pt electrode. A 1:1:1:1:1:1 signal of DMPO-$\cdot O_2^-$ is observed on Si-SnO_2-TiO_x electrode, proving $\cdot O_2^-$ radicals are generated on the electrode.

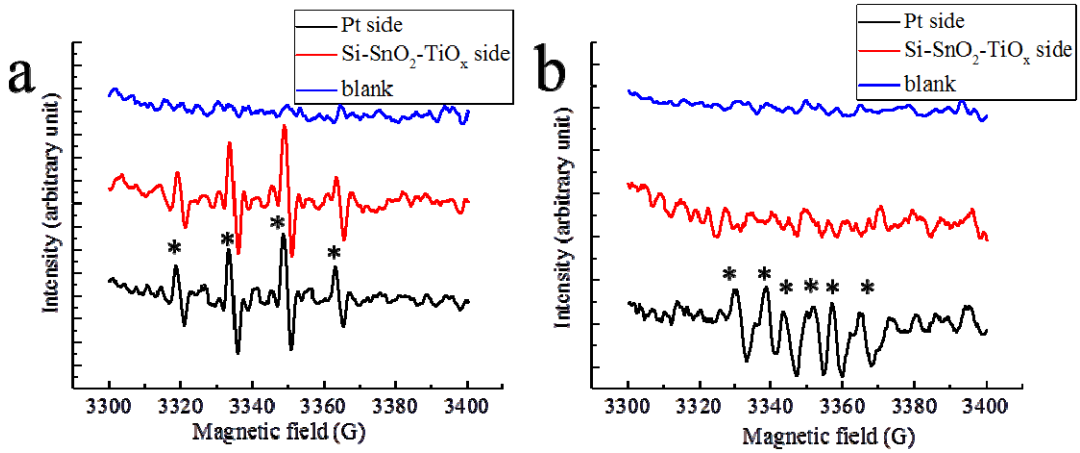

Fig. S7 DMPO spin-trapping ESR spectra of (a) DMPO-·OH and (b) DMPO-·O_2^- in Pt cell and Si-SnO_2-TiO_x cell under simulate solar irradiation

Atrazine and BPA are also applied as simulate pollutants to investigate the degradation ability (Fig. S8). 54% atrazine and 73% BPA could be degraded at zero potential. The rate constants follow pseudo-first-order kinetics. The rate constants of atrazine and BPA degradation at zero potential are 0.237 h^{-1} (R^2 = 0.996) and 0.407 h^{-1} (R^2 = 0.995), respectively.

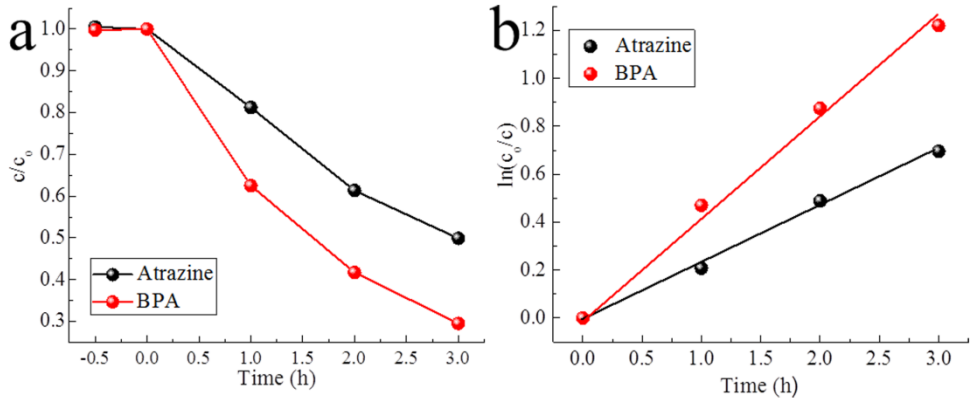

Fig. S8 (a) Atrazine and BPA degradation and (b) kinetic curves of the degradation process

Mott-Schottky measurements of TiO_x and SnO_2 are performed with a bias of 1.0 V to -1.0 V vs. NHE and a frequency of 1 kHz. Flat-band potentials (V_{fb}) are measured as shown in Fig. S9.

V_{fb} of TiO_x is -0.05 V vs. NHE and V_{fb} of SnO_2 is -0.11 V vs. NHE. The value of V_{fb} could be regarded as Fermi level energy.

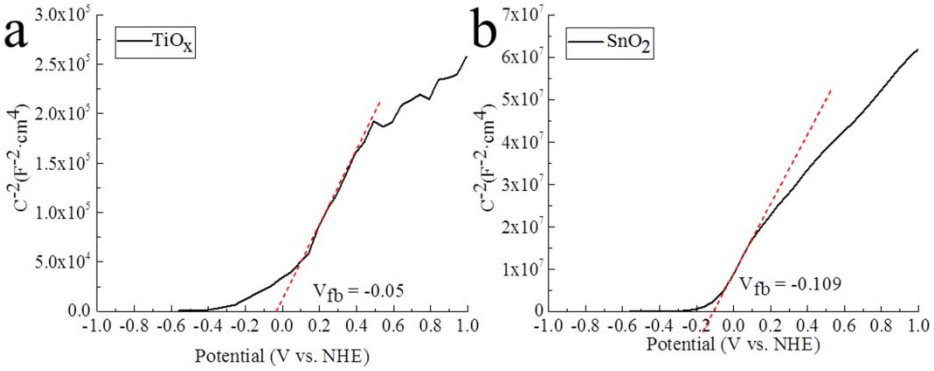

Fig. S9 Mott-Schottky measurements of (a) TiO_x and (b) SnO_2

The valence band of TiO_x is measured by the valence band XPS to confirm the energy band positions, as shown in Fig. S10. TiO_x displays a VB with the edge of the maximum energy at about 2.5 eV.

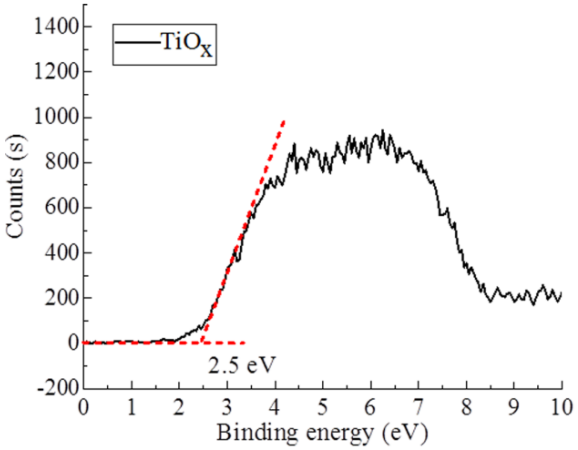

Fig. S10 Valence-band XPS of TiO_x

Fig. S11 reports the UV-vis absorption spectra of TiO_x. Tauc plot method is used to obtain the indirect band gap. Calculated indirect band gap is 3.1 eV.

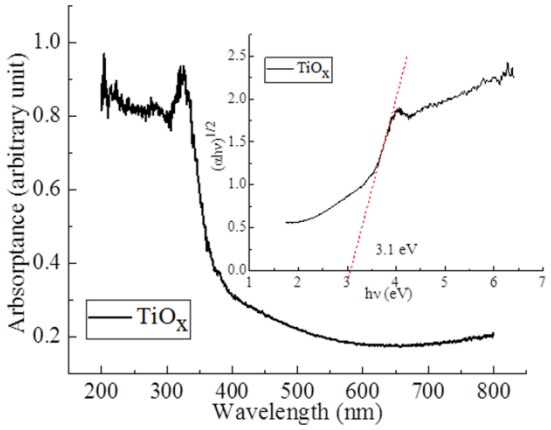

Fig. S11 DRS pattern and Tauc plot (insert figure) of TiO_x

Chopped photocurrent response, cyclic voltammetry test, transient photocurrent response and V_{oc} of Si-Ag-TiO_x are presented in Fig. S12 and all of the performances are much poorer compared to Si-SnO_2-TiO_x.

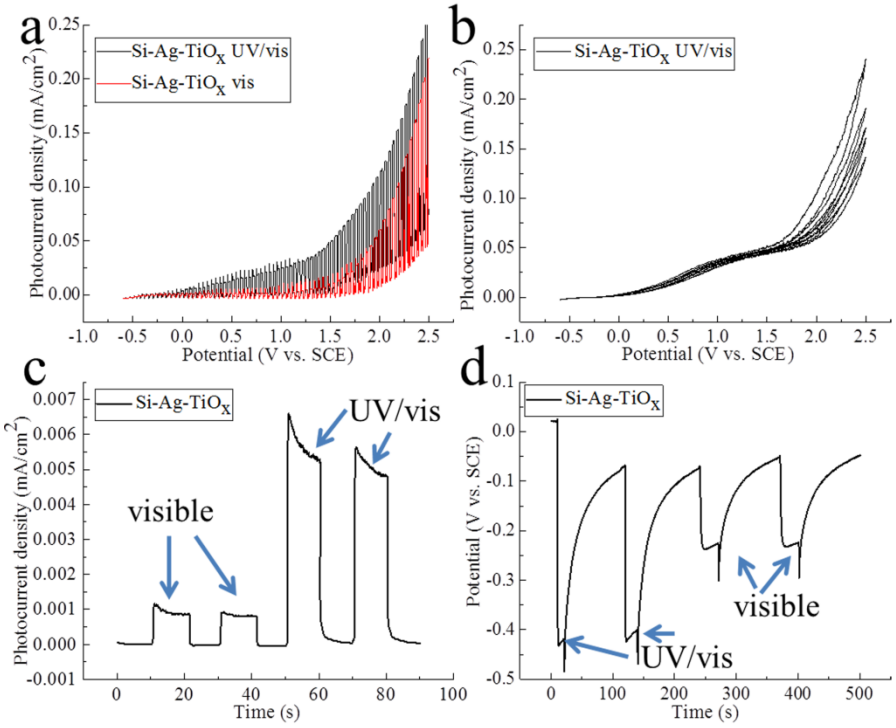

Fig. S12 (a) Chopped photocurrent response, (b) cyclic voltammetry test, (c) photocurrent response and (d) V_{oc} test of Si-Ag-TiO_x

The positions of different valence states of Ti (Ti^{4+}, Ti^{3+} and Ti^{2+}) $2p_{1/2}$ and $2p_{3/2}$ are presented in table S1.

Table S1. The peak positions of different valence states of Ti

Element	**$2p_{1/2}$**	**$2p_{3/2}$**	**Splitting distance**
Ti^{2+}	461.1 eV	455.4 eV	5.7 eV
Ti^{3+}	462.7 eV	457.1 eV	5.6 eV
Ti^{4+}	464.3 eV	458.7 eV	5.6 eV